STM JOURNALS

Journal of
Materials & Metallurgical Engineering

ISSN: 2231-3818 (Online)
ISSN: 2321-4236 (Print)
Volume 16, Issue 2, 2026
May–August
DOI (Journal): 10.37591/JoMME

https://journals.stmjournals.com/jomme

Research JoMME

Structural, Morphological, Optical, and Electrical Properties of Sol–Gel Synthesized Bismuth Ferrite Nanoparticles for Photovoltaic Applications

Samiul Islam[1], Fabliha Sadat Deen[2], Maeesha Ryaan[2], Sikdar Takibul Islam[2], Naime Sarkar[2], M.M. Rhaman[3,*]

Abstract

Solar cells are a promising renewable energy source, converting solar energy into electrical power. The performance and efficiency of solar cells can be enhanced by incorporating multiferroic materials, which have the potential to improve energy conversion. Bismuth ferrite (BFO) is one such material that has attracted attention for photovoltaic applications due to its bandgap energy, which ranges from 2 eV to 2.7 eV. However, its practical efficiency is currently low (less than 2%), limiting its commercial viability. Nevertheless, BFO remains a promising candidate for photovoltaic applications, provided that its properties are optimized. In this study, BFO nanoparticles were synthesized using the sol–gel method, a widely used technique for preparing high-quality nanomaterials. The crystal structure of the synthesized BFO nanoparticles was analyzed using x-ray diffraction (XRD), which revealed a well-defined crystalline structure typical of BFO. The grain morphology of the nanoparticles was examined using field emission scanning electron microscopy (FESEM), providing insights into the particle size and shape. The synthesis process was optimized, and symmetrical-shaped particles were obtained at a calcination temperature of 600°C. The bandgap energy of the BFO nanoparticles was determined to be 2.00 eV for the indirect transition and 2.04 eV for the direct transition, which is suitable for photovoltaic applications. These results indicate that BFO nanoparticles have the potential to be utilized in solar cells, and with further optimization, their efficiency could be improved. This work contributes to the understanding of BFO's structural and optical properties and highlights its potential for use in future photovoltaic devices.

Keywords: Bismuth ferrite nanoparticles, sol–gel synthesis, x-ray diffraction, bandgap energy, photovoltaic materials

***Author for Correspondence**
M.M. Rhaman
E-mail: mizan.eee@aust.edu

[1]Research Assistant, Department of Electrical and Electronic Engineering, Ahsanullah University of Science and Technology, Dhaka, Bangladesh
[2]Graduate Research Scholar, Department of Electrical and Electronic Engineering, Ahsanullah University of Science and Technology, Dhaka, Bangladesh
[3]Professor, Department of Electrical and Electronic Engineering, Ahsanullah University of Science and Technology, Dhaka Bangladesh

Received Date: May 18, 2026
Accepted Date: May 25, 2026
Published Date: June 22, 2026

Citation: Samiul Islam, Fabliha Sadat Deen, Maeesha Ryaan, Sikdar Takibul Islam, Naime Sarkar, M.M. Rhaman. Structural, Morphological, Optical, and Electrical Properties of Sol–Gel Synthesized Bismuth Ferrite Nanoparticles for Photovoltaic Applications. Journal of Materials & Metallurgical Engineering. 2026; 16(2): 28–41p.

INTRODUCTION

The demand for energy across the globe has risen dramatically in recent decades, driven primarily by the accelerating growth of the human population, industrialization, and technological advancements. As global urbanization continues, the corresponding increase in energy consumption presents a critical challenge for governments, industries, and consumers. With this ever-expanding energy demand, ensuring a sustainable energy future has become one of the most significant global concerns worldwide. Simultaneously, the environmental consequences of traditional energy production methods, particularly the reliance on fossil fuels, have prompted urgent discussions on transitioning to more sustainable alternatives. Fossil fuel-based

energy sources, including coal, oil, and natural gas, continue to dominate the global energy landscape, accounting for approximately 80–87% of the global primary energy mix [1, 2]. However, this extensive reliance on fossil fuels contributes significantly to the depletion of finite natural resources and exacerbates the detrimental effects of climate change through the emission of carbon dioxide (CO_2) and other greenhouse gases [3].

Environmental degradation caused by the combustion of fossil fuels is one of the most pressing concerns of the modern age. The rise in global temperatures, depletion of the ozone layer, rising sea levels, and extreme weather events are just a few of the many adverse effects attributed to the unrestrained use of fossil fuels. As the impacts of climate change continue to intensify, a transformation in the global energy sector is imperative. Consequently, there has been a widespread shift toward renewable energy sources, which offer cleaner and more sustainable alternatives to fossil fuels. Renewable energy sources, such as solar, wind, geothermal, and hydropower, are not only environmentally friendly but also inexhaustible, making them crucial for meeting long-term energy needs. Among these, solar energy is one of the most promising and widely applicable alternatives [4, 5].

Solar energy, harnessed from the sun, is abundant, clean, renewable, and sustainable. The sun provides an immense and virtually limitless source of energy, delivering more energy to the Earth in one hour than the entire global population consumes in a year. The ability to convert sunlight into usable electrical power is an alluring prospect for meeting global energy needs, especially because solar energy is widely distributed and can be accessed virtually anywhere on Earth [6–8]. However, the efficiency of solar energy conversion systems, specifically photovoltaic (PV) cells, has been a topic of intense research and development for decades.

Currently, the most widely used photovoltaic technology is the crystalline silicon solar cell. These cells, made from silicon semiconductors, have been commercialized for several decades and have proven reliable, efficient, and relatively cost-effective. Silicon solar cells typically have a bandgap of approximately 1.1 eV, which is optimal for converting sunlight into electricity [9, 10]. Consequently, silicon-based solar cells can achieve solar energy conversion efficiencies of up to 26%, which is the highest efficiency among commercial solar technologies. The performance of these cells is primarily dictated by the ability of silicon to absorb and convert solar energy into electrical power, with approximately 33.33% of solar energy captured by silicon-based photovoltaic devices [11–16].

Although silicon solar cells have dominated the market, they are not without drawbacks. One of the main challenges associated with silicon solar cells is their high production and installation costs [4]. The process of manufacturing silicon wafers, which requires high-temperature processes and complex purification techniques, is energy-intensive and expensive [17–19]. Additionally, the installation of silicon-based solar panels entails significant infrastructure costs. As the global demand for solar energy continues to rise, it is increasingly important to explore alternative materials and technologies that offer lower production costs, improved efficiency, and enhanced functionality [20].

In response to the limitations of silicon-based solar cells, researchers have begun investigating alternative materials and technologies for solar energy conversion applications. Among the most promising candidates are amorphous silicon, quantum dot solar cells, dye-sensitized solar cells (DSSCs), and organic-inorganic perovskite solar cells (PSCs). These materials offer a range of potential benefits, including lower production costs, the ability to absorb a broader range of the solar spectrum, and more versatile manufacturing techniques. As these emerging technologies continue to mature, they are expected to complement and, in some cases, surpass traditional silicon solar cells in terms of both cost and performance [21, 22].

One material that has recently garnered significant attention for its potential photovoltaic applications is bismuth ferrite ($BiFeO_3$) (BFO). BFO is a unique multiferroic material that exhibits

both ferroelectric and magnetic properties at room temperature [23, 24]. Unlike traditional photovoltaic materials, which primarily focus on electronic properties such as bandgap energy and charge carrier mobility, BFO offers the possibility of exploiting its ferroelectric and magnetic ordering to enhance its photovoltaic performance. This combination of properties, particularly the coupling between the magnetic and electronic dipoles, provides unique opportunities for designing novel photovoltaic devices that capitalize on magnetoelectric effects [25].

Bismuth ferrite ($BiFeO_3$) is a lead-free piezoelectric material that has shown great promise for use in photovoltaic (PV) cells owing to its ability to exhibit multiferroic properties at ambient temperature. Multiferroic materials, such as BFO, can exhibit both ferroelectricity (spontaneous polarization that can be reversed by an external electric field) and magnetism (spontaneous magnetization that can be reversed by an external magnetic field) simultaneously. This dual-property nature enables the material to interact with both electric and magnetic fields, resulting in a phenomenon known as the magnetoelectric effect. The ability of BFO to respond to both electric and magnetic fields offers a new way to manipulate and control its properties, making it an attractive candidate for a wide range of applications, including sensor devices, actuators, and non-volatile memory [26, 27].

The Curie temperature (Tc = 1103 K) and Néel temperature (TN = 643 K) of BFO are significantly higher than room temperature, making it suitable for high-temperature applications. The ferroelectric properties of the material are driven by the 6s lone pair electrons of Bi^{3+} ions, whereas the Fe^{3+} ions contribute to the magnetic ordering. These unique structural and electronic characteristics make BFO an intriguing material for photovoltaic devices. Furthermore, the bandgap of BFO, ranging from 2.0 to 2.7 eV, places it in the optimal range for absorbing visible light, which further enhances its suitability for solar energy conversion.

However, despite the significant promise of BFO for photovoltaic applications, several challenges remain. One of the main barriers to its widespread use is its high resistivity, which impedes the efficient flow of electrical currents [28, 29]. Additionally, leakage current and the formation of impurity phases within the material can reduce the overall efficiency of BFO-based photovoltaic devices. [30]. However, these challenges are not insurmountable. Research has shown that doping and co-doping BFO with various elements, such as rare earth elements (e.g., Sm, Eu, and Gd) and transition metals (e.g., Cr, Mn, and Co), can improve its electrical conductivity and reduce the formation of undesirable phases. These modifications can also enhance the dielectric properties and optimize the bandgap energy, further improving the potential of the material for use in high-efficiency solar cells [31–36].

Research on bismuth ferrite (BFO) as a photovoltaic material is still in its early stages, but it holds considerable promise. As researchers continue to explore the potential of multiferroic materials in solar energy applications, BFO is likely to play a significant role in the development of next generation photovoltaic technologies. The ability to manipulate both the electric and magnetic properties, coupled with the potential for doping and co-doping to optimize performance, makes BFO a highly versatile material for future solar cell designs. Furthermore, the low toxicity and lead-free nature of BFO make it an environmentally friendly alternative to other photovoltaic materials, such as PSCs, which contain toxic elements such as lead [37, 38].

In conclusion, ongoing advancements in materials science and engineering offer exciting prospects for improving the efficiency and cost-effectiveness of solar energy systems. Bismuth ferrite (BFO) stands out as one of the most promising materials for the next generation of photovoltaic devices, owing to its unique combination of ferroelectric and magnetic properties, bandgap energy, and the potential for optimization through doping. With continued research and development, BFO-based solar cells could provide an environmentally friendly, efficient, and cost-effective solution to the global energy crisis. [39–41].

MATERIALS AND METHODS

Bismuth ferrite ($BiFeO_3$) nanoparticles were synthesized using a modified Pechini sol–gel method. Initially, bismuth nitrate pentahydrate ($Bi(NO_3)_3 \cdot 5H_2O$) and iron nitrate nonahydrate ($Fe(NO_3)_3 \cdot 9H_2O$) were dissolved in 400 mL of deionized water to prepare a 0.025 M solution of each. After stirring for 30 min, citric acid (0.02 mol) was added as a chelating agent, which facilitated the complexation of the metal cations. The solution was heated at 70–75°C for 8–10 hours, forming a transparent blackish-red sol. To control the pH, ammonium hydroxide (NH_4OH) was added dropwise, maintaining the pH within the range of 1–2. Next, ethylene glycol was added to initiate the polymerization reaction, and the solution was heated at 85–90°C, leading to the formation of a gel. The gel was then dried at 100°C for 24 h to obtain a green xerogel. To enhance the homogeneity of the nanoparticles, the xerogel was annealed at 600°C for 2 h in static air, with a furnace heating and cooling rate of 3°C/min. For bulk $BiFeO_3$ production, another xerogel sample was annealed at 800°C. Impurity phases were removed by washing the powders with acetic acid and deionized water at 70°C. The final nanoparticles were dried for subsequent characterization. This modified process, which uses deionized water as the solvent and citric acid as a stronger chelating agent, yields more homogeneous and well-defined $BiFeO_3$ nanoparticles than the initial sol–gel method. The detailed sol–gel procedure has been provided elsewhere [42]. Figure 1 shows a flowchart of the sol–gel synthesis procedure. In this study, a two-step synthesis route combining sol–gel processing and auto-combustion techniques was employed to examine how the synthesis method influences the structural and functional properties of BFO nanoparticles.

X-ray powder diffraction (XRD) is a widely used analytical technique for determining the crystalline structure, phase composition, and lattice parameters of a material. In this study, XRD analysis was performed at room temperature using a PANalytical Empyrean X-ray diffractometer.

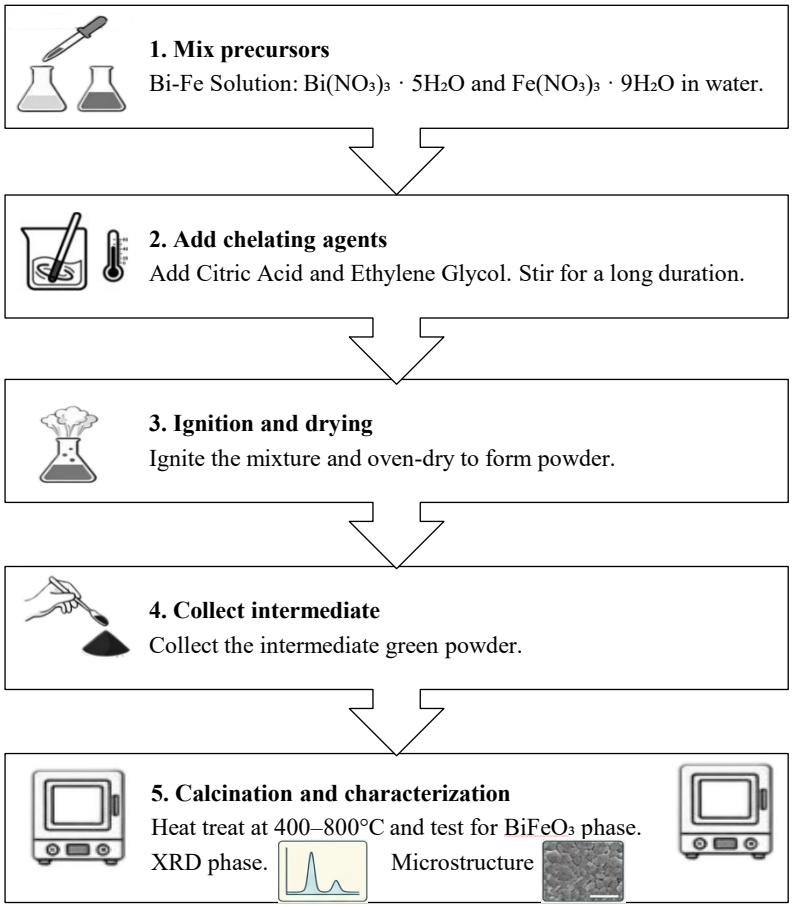

Figure 1. Flow chart of the synthesis procedure of BFO nanoparticles using the non-auto combustion sol–gel method.

RESULTS AND DISCUSSION

X-Ray Diffraction

The diffraction patterns of the bismuth ferrite ($BiFeO_3$) nanoparticles were obtained by scanning the samples over a 2θ range of 10° to 70° with high-intensity X-ray beams. The XRD patterns of $BiFeO_3$ nanoparticles annealed at 600°C were recorded before and after washing with acetic acid (CH_3COOH). Acetic acid, a weak acid, was used to remove impurity phases while preserving the crystallinity of the nanoparticles. The XRD analysis shown in Figure 2 confirmed that the nanoparticles retained their crystalline structure, as evidenced by the well-defined diffraction peaks corresponding to the rhombohedral perovskite structure of $BiFeO_3$. The XRD patterns of the nanoparticles were consistent with the expected crystallographic features of $BiFeO_3$, indicating successful synthesis and phase formation at the annealing temperature. Furthermore, the minimal alteration in the XRD patterns after washing with acetic acid suggests that the washing procedure did not significantly affect the crystallinity of the material. The atomic coordinates of the rhombohedral surfaces of $BiFeO_3$ were used to optimize the atomic structure coordination, providing further confirmation of the crystallinity of the material. In addition to the dominant R3c perovskite phase, a few very low-intensity peaks corresponding to minor secondary phases, such as $Bi_2Fe_4O_9$ and $Bi_{25}FeO_{40}$, were observed, which is consistent with previous reports [43–47]. In this study, the reflections associated with $Bi_2Fe_4O_9$ are specifically marked with an asterisk (*) in the XRD patterns to clearly distinguish them from the primary phase. Importantly, the extremely weak intensity of these peaks highlights the effectiveness of the adopted synthesis route in suppressing the formation of non-perovskite impurity phases, thereby ensuring a high degree of phase purity in BFO nanoparticles. The XRD results validated the formation of high-quality crystalline $BiFeO_3$ nanoparticles, making them suitable for further applications, including photovoltaic and magnetoelectric devices.

FESEM Micrograph Analysis

FESEM is a type of microscope that uses electrons rather than light. FESEM is a field emission scanning electron microscope**.** The field emission source liberates electrons that scan the product in a zigzag pattern. Figure 3 displays the 600°C $BiFeO_3$ micrograph. Nanoparticles found at this temperature were spherical and had a consistent distribution of dimensions [48]. As the temperature increased, the particle size also increased. This coarsening is driven by a reduction in the total surface area induced by the increase in the average particle size. In this process, it is difficult to achieve a uniform particle size distribution. The vapor pressure is higher on smaller particles than on coarser particles at high temperatures, and they condense into larger particles.

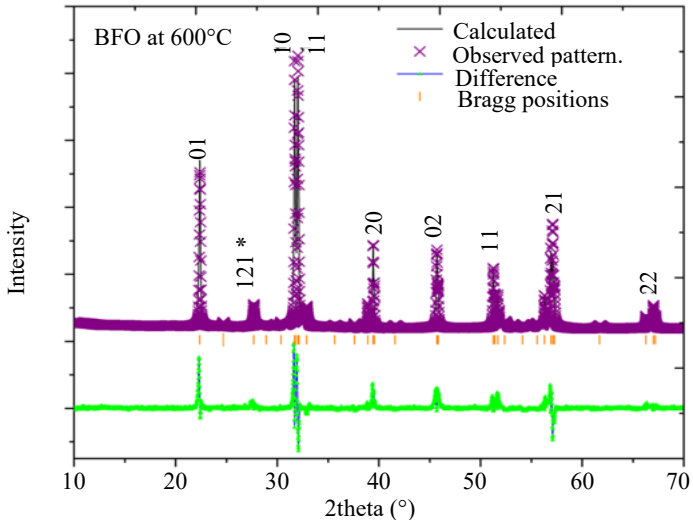

Figure 2. XRD analysis at 600°C confirmed that $BiFeO_3$ nanoparticles retained their crystalline structure.

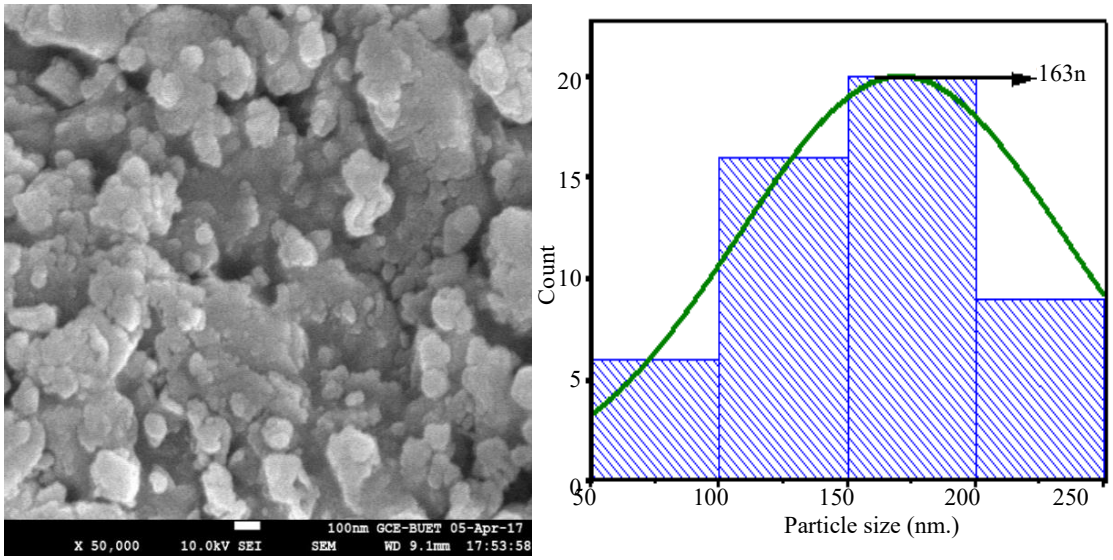

Figure 3. Field emission scanning electron microscope morphology (FESEM) of BFO nanoparticles at 600°C.

The particle sizes obtained from the FESEM micrographs and XRD data are comparable. Consequently, the nanoparticles were monocrystalline. The crystal size obtained from the XRD data was smaller than the particle size obtained from the FESEM images. As nanoparticles have a smaller volume-to-surface area ratio, these tendencies cause them to clump and cause multiple crystallites to be added to a particle [49–52].

Bandgap Engineering

The small bandgap energy (E_g) of BFO makes it an efficient visible light irradiator. The PV absorption capacity of BFO is closely connected to its electronic structure and is regarded as a significant element in calculating the energy gap between its bands [53, 54]. The optical E_g of BFO was measured using a UV–Vis–NIR Spectrophotometer (Model: PerkinElmer UV–Vis–NIR Spectrometer Lambda 1050) using diffuse reflectance spectra. In Kubelka-Munk's work, the diffuse reflectance information was converted as follows:

$$F(R) = \frac{(1-R)^2}{2R} \quad (1)$$

Here, the diffuse reflectance is R. Here, firstly, we obtained the values of E_g for pure BFO at a temperature of 600°C. The material receives sufficient energy to drive electrons out of its weak connection by solar radiation with wavelengths ranging from 380 to 750 nm (violet to red). This results in electrical current generation. The unutilized wavelengths, ultraviolet (10 to 380 nm) and infrared (750 to 1000,000 nm), are insufficient to release and absorb electrons as heat. For data collection, a range of waves from 200 to 800 nm was considered.

Figure 4 presents the direct and indirect bandgap analyses of pure BFO annealed at 600°C. The corresponding bandgap energy (Eg) values obtained for the pure BFO sample at this annealing temperature are shown in Figure 4. The bandgap energy is shown at the crossing point of the tangent line $[F(R)hv]^2 = 0$. The energy (eV) difference between the valence band (VB) (O 2p) and the conduction band (CB Fe 3d) is thus similar to that of BFO. The E_g value depends on the particle size [55–57]. The Eg is lowered if the particle size is small. The Fe-O bond length and the bond angle Fe–O–Fe were exchanged. The test equation indicates the bond length and angle of connection W:

$$W \propto \frac{\cos\omega}{d_{Fe-O}^{3.5}} \quad (2)$$

where $\omega = 1/2\{\pi - (Fe\text{-}O\text{-}Fe)\}$ and $d_{Fe\text{-}o}$ is the Fe–O bond length. E_g is linked to W. For example:

$$E_g = \Delta - W \quad (3)$$

where Δ is the invariant charge transfer energy. The Fe–O bond length of the connection is also substantially lower than that in the rhombohedral phase. The average bond duration of Fe–O increases with increasing temperature, and Fe–O–Fe decreases with the bond angle [58, 59]. Thus, E_g raises the BFO temperature.

The relationship between the direct bandgap and particle size is shown in Figure 5. The value of E_g depends on the size of the BFO particles. If the size of the BFO particle is larger, the band gap energy E_g will increase, and if the size of the BFO particle is smaller, the band gap energy E_g will decrease, as shown in Table 1.

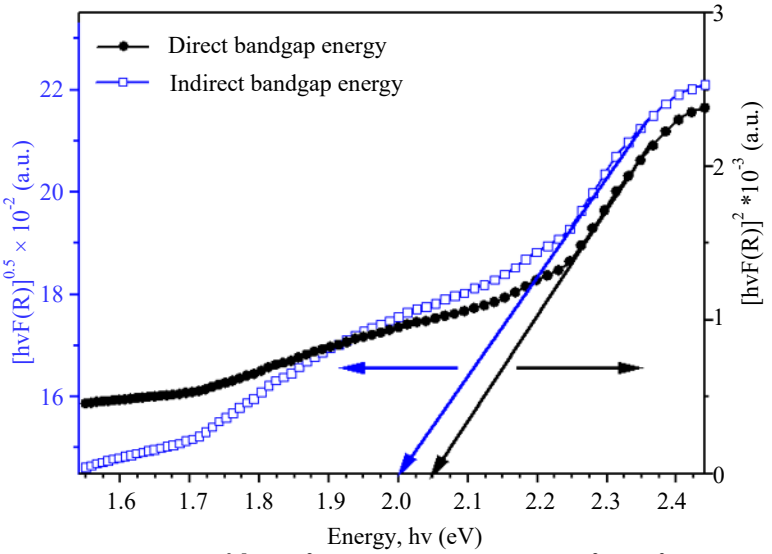

Figure 4. $[hvF(R)]^{0.5} *10^{-2}$ versus E, and $[hvF(R)]^2 *10^{-3}$ versus E from BFO, annealed at 600°C.

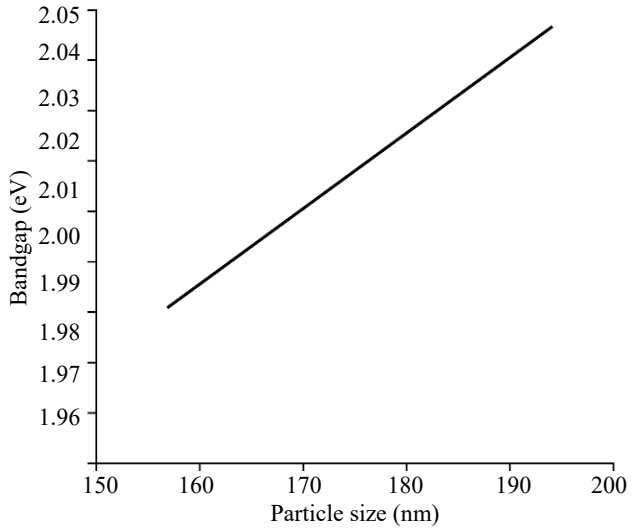

Figure 5. Relation between bandgap (direct) and particle size.

Table 1. $BiFeO_3$ samples of particles and bandgaps annealed at various temperatures.

BFO annealing temperature (°C)	Particle size (nm)	Bandgap (eV)	
600	163	2.04 (direct)	2.00 (indirect)

Optical Band Gap and Electrical Properties

The bandgap energy (Eg) represents the energy difference between the top of the valence band and the bottom of the conduction band in a solid material [60, 61]. No electronic states are available in this energy region. Optical absorption occurs when incident photons possess sufficient energy to excite electrons from the valence band to the conduction band. Therefore, the band gap plays an important role in determining the light absorption ability of a material. Materials with comparatively higher band gap energies absorb a smaller portion of the solar spectrum, whereas materials with suitable band gap values are more effective for photovoltaic applications [62–64].

The electrical properties of the $BiFeO_3$ nanoparticles shown in Figure 6, including resistance, reactance, impedance, and AC conductivity, were investigated as a function of frequency at room temperature. The frequency-dependent resistance, reactance, and impedance were measured over the range of 20 Hz to 10 MHz, while the AC conductivity was analyzed within the selected high-frequency region. The variations in the resistance, reactance, and impedance exhibited similar behaviors with increasing frequency. At lower frequencies, the values decreased sharply, indicating a strong frequency dependence. The response can be divided into three regions: first, a rapid decrease in the resistive component between 20 Hz and 10^2 Hz; second, a gradual decrease between 10^2 Hz and 10^3 Hz; and third, a nearly stable response above 10^3 Hz. Figure 6(a) shows the response of the resistance.

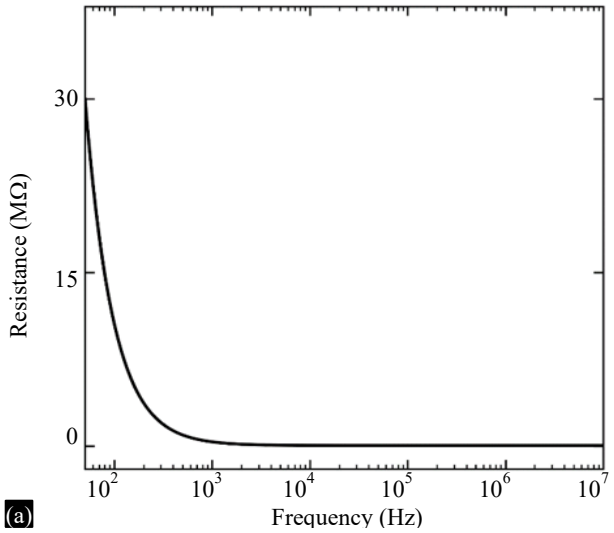

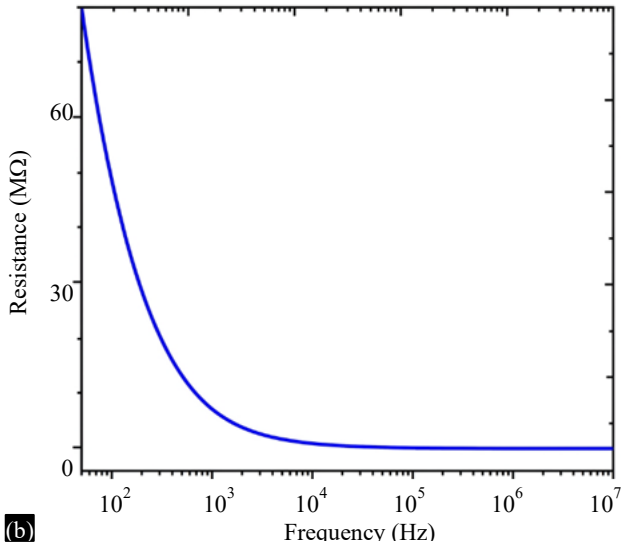

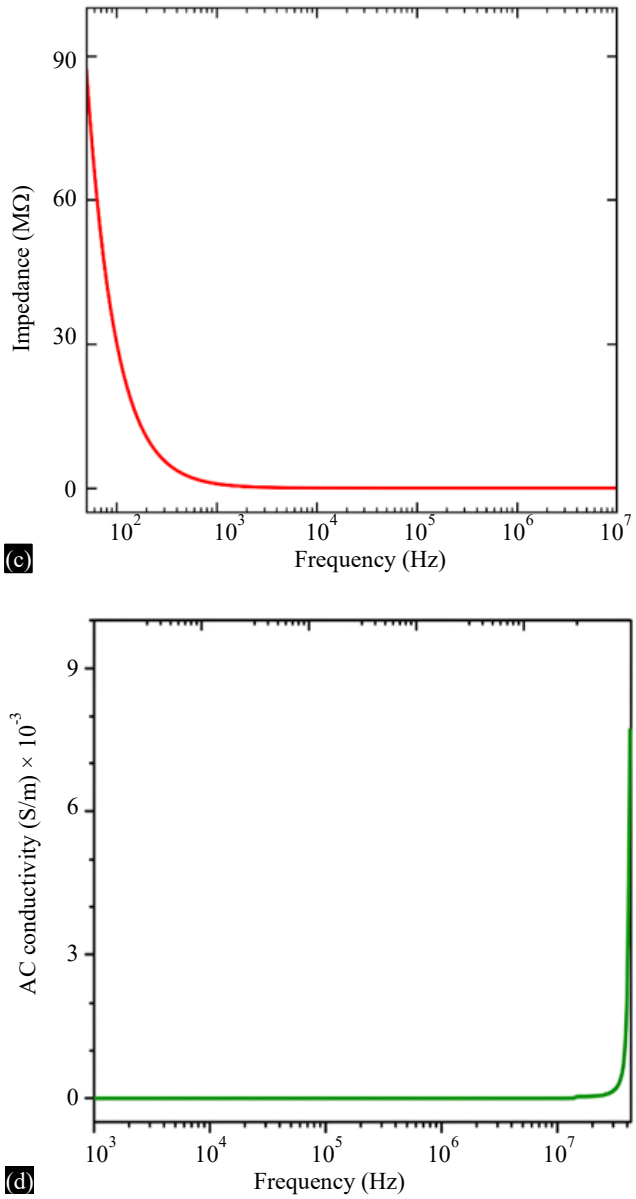

Figure 6. Electrical properties of BFO nanoparticle samples: (a) resistance, (b) reactance, (c) impedance, and (d) AC conductivity.

The sharp decrease in resistance at low frequencies may be associated with space charge polarization and charge accumulation at the grain boundaries [26]. At higher frequencies, the resistance became almost constant, suggesting that the accumulated charges could not follow the rapidly changing external electric field. In Figure 6(b), a similar decreasing trend was observed for the reaction, which may be attributed to the enhanced charge carrier hopping and improved AC conduction at higher frequencies. The reduction in reactance also indicates a lower opposition to alternating current flow within the material [65].

Figure 6(c) shows that the impedance of the BFO nanoparticles also decreased significantly with increasing frequency, particularly below 1 kHz. This behavior indicates a reduction in the resistive barriers and an improvement in the conductivity. With increasing dopant concentration, the resistance, reactance, and impedance decreased, suggesting improved electrical conductivity of the samples, as shown in Figure 6(d). The decrease in grain size with doping may also contribute to changes in the grain boundary behavior and charge transport mechanisms [66–69].

Overall, the frequency-dependent electrical response of the BFO nanoparticles confirmed their semiconducting behavior and highlighted the role of grain boundaries, space charge polarization, and charge carrier hopping in determining their electrical performance. These properties are important for evaluating the suitability of BFO nanoparticles for photovoltaic and other electronic applications [70–73].

CONCLUSION

This study aimed to explore the structural and electrical properties of bismuth ferrite ($BiFeO_3$) nanoparticles for potential applications in photovoltaic devices. $BiFeO_3$ nanoparticles were successfully synthesized using a soft-chemical method. Optical analysis revealed bandgap energies of 2.00 eV for the indirect transition and 2.04 eV for the direct transition, indicating the semiconducting nature of the synthesized BFO nanoparticles and their potential suitability for optoelectronic and photovoltaic applications. The bandgap was found to be 2.04 eV, which is close to the optimal range for photovoltaic applications (typically around 1.5 eV). The structural characterization of the nanoparticles was performed using XRD and field emission scanning electron microscopy (FESEM), both of which confirmed the successful synthesis of crystalline $BiFeO_3$ nanoparticles with a well-defined perovskite structure. The XRD patterns revealed the expected crystalline phases, whereas FESEM imaging revealed a uniform particle distribution, indicating the effectiveness of the synthesis method. Given its suitable bandgap and crystallinity, $BiFeO_3$ holds significant promise for solar cell applications. The results of this study suggest that $BiFeO_3$ nanoparticles, with further optimization of the synthesis parameters, could be a viable alternative to conventional photovoltaic materials, offering a promising path for developing efficient and cost-effective solar cells. This study paves the way for future research aimed at enhancing the photovoltaic performance of $BiFeO_3$ through doping, surface modifications, and improved fabrication methods.

REFERENCES

1. Sever SD. Climate change and the energy transition in the MENA region. In: Climate Change Law and Policy in the Middle East and North Africa Region. Abingdon (UK): Routledge; 2021. p.82-106. doi:10.4324/9781003044109-6.
2. Rhaman MM. Hybrid renewable energy system for sustainable future of Bangladesh. Int J Renew Energy Res. 2013;3(4):777-780.
3. Tanvir RU, Shahadat MR, Ghosh M, Khan M. Prospects and utilization of renewable energy in Bangladesh: A review article. Int J Sci Eng Res. 2017;8(4):490-491.
4. Rhaman MM. A remarkable cost-effective solar home system in rural area of Bangladesh. Curr Altern Energy. 2018;2(1):37-41. doi:10.2174/2405463103666180402143554.
5. Roy S, Rhaman MM. Hybrid solar power plant in Saint Martin's island can enlarge tourist attraction in Bangladesh. Int J Eng Manuf. 2016;6:12-22. doi:10.5815/ijem.2016.03.02.
6. Rhaman MM, Islam S. On-grid renewable energy system design and cost analysis with Homer software for Aust. computer (desktop), 700, 70. [Incomplete bibliographic information.]
7. Rhaman MM. Solar base renewable energy for a sustainable future in Bangladesh. In: Proceedings of the 4th Global Engineering, Science and Technology Conference. p.27-28.
8. Shukla AR, Skea J, Reisinger AI, Slade R, Fradera R, Pathak M, et al. Summary for policymakers. In: Climate Change: Mitigation of Climate Change. Contribution of Working Group III to the Sixth Assessment Report of the Intergovernmental Panel on Climate Change. Geneva: Intergovernmental Panel on Climate Change; 2022. p.3-48.
9. Rhaman MM. Recent advances of light emitting diode for solid state lighting. In: Proceedings of the 10th Global Engineering, Science and Technology Conference. Dhaka: BIAM Foundation; 2015. p.2-3.
10. Rhaman MM, Matin MA, Toshon TA. Solid state lighting can resolve the present power crisis in Bangladesh. In: 3rd International Conference on Green Energy and Technology (ICGET); 2015. p.1-5. doi:10.1109/ICGET.2015.7315100.

11. Green M, Dunlop E, Hohl-Ebinger J, Yoshita M, Kopidakis N, Hao X. Solar cell efficiency tables (version 57). Prog Photovolt Res Appl. 2021;29(1):3-15. doi:10.1002/pip.3371.
12. Ru X, Yang M, Yin S, Wang Y, Hong C, Peng F, et al. Silicon heterojunction solar cells achieving 26.6% efficiency on commercial-size p-type silicon wafer. Joule. 2024;8:1092-1104. doi:10.1016/j.joule.2024.01.015.
13. Luque A, Sala G, Palz W, Dos Santos G, Helm P, editors. Proceedings of the International Conference, Held at Lisbon, Portugal: Tenth EC Photovoltaic Solar Energy Conference. Berlin: Springer; 1991. [Source contains inconsistent publication information: "p. 2012 Dec 6."]
14. Pastuszak J, Węgierek P. Photovoltaic cell generations and current research directions for their development. Materials. 2022;15(16):5542. doi:10.3390/ma15165542. PMID:36013679.
15. Rhaman MM, Matin MA, Hakim MA, Islam MF. Dielectric, ferroelectric and ferromagnetic properties of samarium doped multiferroic bismuth ferrite. Mater Res Express. 2019;6(12):125080. doi:10.1088/2053-1591/ab57c2.
16. Rhaman MM, Matin MA. Organic solar cells: Historical developments and challenges. In: 2015 International Conference on Advances in Electrical Engineering (ICAEE); 2015. p.26-29. doi:10.1109/ICAEE.2015.7506788.
17. Yu Y, Bai X, Li S, Shi J, Wang L, Xi F, et al. Review of silicon recovery in the photovoltaic industry. Curr Opin Green Sustain Chem. 2023;44:100870. doi:10.1016/j.cogsc.2023.100870.
18. Ballif C, Haug FJ, Boccard M, Verlinden PJ, Hahn G. Status and perspectives of crystalline silicon photovoltaics in research and industry. Nat Rev Mater. 2022;7(8):597-616. doi:10.1038/s41578-022-00423-2.
19. Hoover H, Bell R, Rippy K. Emerging technologies for decarbonizing silicon production. J Sustain Metall. 2024;10(4):1921-1932. doi:10.1007/s40831-024-00913-3.
20. Woodhouse MA, Smith B, Ramdas A, Margolis RM. Crystalline silicon photovoltaic module manufacturing costs and sustainable pricing, 1h (2018). Benchmark and Cost Reduction Road Map. Golden (CO): National Renewable Energy Laboratory, Office of Energy Efficiency and Renewable Energy; 2019 Feb 14.
21. Rhaman MM, Matin MA, Hossain MN, Khan MNI, Hakim MA, Islam MF. Ferromagnetic, electric, and ferroelectric properties of samarium and cobalt co-doped bismuth ferrite nanoparticles. J Phys Chem Solids. 2020;147:109607. doi:10.1016/j.jpcs.2020.109607.
22. Rhaman MM, Matin MA, Al Mamun MA, Hussain A, Hossain MN, Das BC, et al. Enhanced electrical conductivity and multiferroic property of cobalt-doped bismuth ferrite nanoparticles. J Mater Sci Mater Electron. 2020;31(11):8727-8736. doi:10.1007/s10854-020-03407-6.
23. Rhaman MM, Matin MA, Hossain MN, Mozahid FA, Hakim MA, Rizvi MH, et al. Bandgap tuning of Sm and Co co-doped BFO nanoparticles for photovoltaic application. J Electron Mater. 2018;47:6954-6958. doi:10.1007/s11664-018-6597-7.
24. Selbach SM, Tybell T, Einarsrud MA, Grande T. Size-dependent properties of multiferroic BiFeO3 nanoparticles. Chem Mater. 2007;19:6478-6484. doi:10.1021/cm071827w.
25. Rhaman MM, Matin MA, Hossain MN, Mozahid FA, Hakim MA, Islam MF. Bandgap engineering of cobalt-doped bismuth ferrite nanoparticles for photovoltaic applications. Bull Mater Sci. 2019;42:190. doi:10.1007/s12034-019-1871-8.
26. Rhaman MM, Matin MA, Hakim MA, Islam MF. Bandgap tuning of samarium and cobalt co-doped bismuth ferrite nanoparticles. Mater Sci Eng B. 2021;263:114842. doi:10.1016/j.mseb.2020.114842.
27. Valant M, Axelsson AK, Alford N. Peculiarities of a solid-state synthesis of multiferroic polycrystalline BiFeO3. Chem Mater. 2007;19(22):5431-5436.
28. Matin MA, Rhaman MM, Hakim MA, Islam MF. Bi(1-y)SmyFeO3 as prospective photovoltaic materials. Bull Mater Sci. 2020;43(1):167. doi:10.1007/s12034-020-02118-2.
29. Kim JK, Kim SS, Kim WJ. Sol-gel synthesis and properties of multiferroic BiFeO3. Mater Lett. 2005;59(29-30):4006-4009. doi:10.1016/j.matlet.2005.07.050.
30. Niloy NR, Chowdhury MI, Anowar S, Islam J, Rhaman MM. Structural and optical characterization of multiferroic BiFeO3 nanoparticles synthesized at different annealing temperatures. J Nano Electron Phys. 2020;12:05015-05011. doi:10.21272/jnep.12(5).05015.

31. Rhaman MM, Matin MA, Hakim MA, Islam MF. Optical and electrical properties of impurity-less multiferroic bismuth ferrite nanoparticles. Mater Sci Eng B. 2022;275:115501. doi:10.1016/j.mseb.2021.115501.
32. Zhang F, Zeng X, Bi D, Guo K, Yao Y, Lu S. Dielectric, ferroelectric, and magnetic properties of Sm-doped BiFeO3 ceramics prepared by a modified solid-state-reaction method. Materials. 2018;11(11):2208. doi:10.3390/ma11112208. PMID:30405047.
33. Do D, Kim JW, Kim SS, Kim WJ, Lee MH, Cho HJ, et al. Reduced leakage current and improved ferroelectric properties of Eu and Mn codoped BiFeO3 thin films. J Korean Phys Soc. 2012;60(2):203-206. doi:10.3938/jkps.60.203.
34. Zhang N, Chen D, Niu F, Wang S, Qin L, Huang Y. Enhanced visible light photocatalytic activity of Gd-doped BiFeO3 nanoparticles and mechanism insight. Sci Rep. 2016;6(1):26467. doi:10.1038/srep26467. PMID:27198166.
35. Taisan NA, Kumar S, Alshoaibi A. Structural, electrical and optical properties of TM (Mn and Cr) doped BiFeO3 nanoparticles. Crystals. 2022;12(11):1610. doi:10.3390/cryst12111610.
36. Naganuma H, Miura J, Okamura S. Ferroelectric, electrical and magnetic properties of Cr, Mn, Co, Ni, Cu added polycrystalline BiFeO3 films. Appl Phys Lett. 2008;93(5). doi:10.1063/1.2965799.
37. Hossain MN, Matin MA, Islam MM, Rhaman MM, Hakim MA, Islam MF. Aspects of structural and multiferroic properties of A-(15% Gd) and B-site (5-15% Cr) doped perovskite BiFeO3 nanoparticles. Trans Electr Electron Mater. 2021;22(4):543-549. doi:10.1007/s42341-020-00264-2.
38. Hossain MN, Matin MA, Rhaman MM, Ali MA, Hakim MA, Roy SK. Structural and dielectric progression of 5% Gd doped BiFeO3 nanoparticles through Cr (2-8%) doping. J Eng Sci. 2022;12(3):101-110. doi:10.3329/jes.v12i3.57483.
39. Rhaman MM, Islam MS, Islam MA. Advancements and challenges of bismuth ferrite-based materials for photovoltaic devices: A study on pure, doped, and co-doped variants. Adv Sci Technol. 2026;175:11-16. doi:10.4028/p-UE9yyx.
40. Rhaman MM, Islam MS, Islam MA, Miah MS, Hasan SK. Phase evolution and dielectric tuning in samarium and cobalt co-doped bismuth ferrite nanoparticles via sol-gel synthesis. J Mater Sci Mater Electron. 2026;37(13):1025. doi:10.1007/s10854-026-17411-9.
41. Mohsin TB, Abidul Islam SM, Tonni TT, Rhaman MM. Analysis of conductivity and band-gap energy of bismuth ferrite nanoparticles as prospective photovoltaic material. Mater Today Proc. 2023. doi:10.1016/j.matpr.2023.01.330.
42. Hedge MS, Aruna ST, Rattan T, Patil KC. Chemistry of Nanocrystalline Oxide Materials: Combustion Synthesis, Properties and Applications. Singapore: World Scientific Publishing; 2008.
43. Rhaman MM, Miah MS, Ahmad T. Investigation of magnetic and electric properties of bismuth ferrite nanoparticles at different temperatures. Nano-Struct Nano-Objects. 2024;39:101304. doi:10.1016/j.nanoso.2024.101304.
44. Matin MA, Rhaman MM, Hossain MN, Mozahid FA, Hakim MA, Rizvi MH, et al. Effect of preparation routes on the crystal purity and properties of BiFeO3 nanoparticles. Trans Electr Electron Mater. 2019;20(6):485-493. doi:10.1007/s42341-019-00140-8.
45. Jaiswal A, Das R, Vivekanand K, Mary Abraham P, Adyanthaya S, Poddar P. Effect of reduced particle size on the magnetic properties of chemically synthesized BiFeO3 nanocrystals. J Phys Chem C. 2010;114(5):2108-2115. doi:10.1021/jp910745g.
46. Rojas-George G, Silva J, Castañeda R, Lardizábal D, Graeve OA, Fuentes L, et al. Modifications in the rhombohedral degree of distortion and magnetic properties of Ba-doped BiFeO3 as a function of synthesis methodology. Mater Chem Phys. 2014;146(1-2):73-81. doi:10.1016/j.matchemphys.2014.02.044.
47. Rhaman MM, Rahman N, Akther S, Islam MA, Hasan SK. Optical and structural property analysis of samarium and cobalt co-doped bismuth ferrite nanoparticles. In: 6th International Conference on Sustainable Technologies for Industry 5.0. Institute of Electrical and Electronics Engineers; 2024. p.1-5. doi:10.1109/STI64222.2024.10951086.

48. Efaz ET, Rhaman MM, Imam SA, Bashar KL, Kabir F, Mourtaza ME, et al. A review of primary technologies of thin-film solar cells. Eng Res Express. 2021;3(3):032001. doi:10.1088/2631-8695/ac2353.
49. Lomanova NA, Osipov AV, Ugolkov VL, Kenges KM, Yastrebov SG. Facile solution combustion synthesis of BiFeO3 nanopowder with improved magnetic and photocatalytic characteristics. Inorg Chem Commun. 2025;178:114591. doi:10.1016/j.inoche.2025.114591.
50. Niloy NR, Chowdhury MI, Shanto MAH, Islam J, Rhaman MM. Multiferroic bismuth ferrite nanocomposites as a potential photovoltaic material. In: IOP Conference Series: Materials Science and Engineering. 2021;1091:012049. doi:10.1088/1757-899X/1091/1/012049.
51. Awni AG, Ali Abbas ZM. Morphological and structural properties of bismuth-nickel ferrite synthesized by a combined sol-gel method. Nexo Rev Cient. 2023;36(6):1076-1086. doi:10.5377/nexo.v36i06.17465.
52. Gil-González E, Perejón A, Sánchez-Jiménez PE, Sayagués MJ, Raj R, Pérez-Maqueda LA. Phase-pure BiFeO3 produced by reaction flash-sintering of Bi2O3 and Fe2O3. J Mater Chem A. 2018;6(13):5356-5366. doi:10.1039/C7TA09239C.
53. Rhaman MM, Matin MA, Hossain NM, Hakim MA, Islam MF. Prospect and barrier of multiferroic bismuth ferrite for application in solar cell. In: 2nd International Conference on Innovation in Engineering and Technology (ICIET); 2019. Institute of Electrical and Electronics Engineers; 2019. p.1-5. doi:10.1109/ICIET48527.2019.9290733.
54. Kebede MT, Dillu V, Devi S, Chauhan S. Phase transition and optical properties of samarium-doped BiFeO3 nanoparticles. J Mater Sci Mater Electron. 2020;31(22):19950-19960. doi:10.1007/s10854-020-04518-w.
55. Matin MA, Hossain MN, Rhaman MM, Mozahid FA, Ali MA, Hakim MA, et al. Dielectric and optical properties of Ni-doped LaFeO3 nanoparticles. SN Appl Sci. 2019;1(11):1479. doi:10.1007/s42452-019-1453-9.
56. Hossain MN, Rhaman MM, Ali MA, Jahan N, Momin AA, Rahman MM, et al. Novel gadolinium (Gd) and chromium (Cr) co-doped yttrium iron garnet (Y3Fe5O12) nanoparticles. Arab J Sci Eng. 2024;49(7):9967-9982. doi:10.1007/s13369-023-08613-y.
57. Catalan G, Scott JF. Physics and applications of bismuth ferrite. Adv Mater. 2009;21(24):2463-2485. doi:10.1002/adma.200802849.
58. Rhaman MM. Comparative sol-gel synthesis approaches for BiFeO3 nanoparticles for photovoltaic solar cell applications. J Adv Mater Eng. 2026;11:1-15. doi:10.46610/JoAME.2026.v11i01.001.
59. Saha S, Routray KL, Nayak TK, Dash B. Effect of synthesis techniques on bismuth ferrite (BiFeO3): An investigative study using structural, optical, and electrochemical performance towards photostability. Braz J Phys. 2024;54(5):147. doi:10.1007/s13538-024-01515-w.
60. Ihlefeld JF, Podraza NJ, Liu ZK, Rai RC, Xu X, Heeg T, et al. Optical band gap of BiFeO3 grown by molecular-beam epitaxy. Appl Phys Lett. 2008;92(14). doi:10.1063/1.2901160.
61. Jindata W, Musikajaroen S, Wongpratat U, Jaisuk C, Wongprasod S, Tanapongpisit N, et al. Enhanced energy density of LiNi0.5Mn0.3Co0.2O2 batteries with negative-electronic-compressibility thin film coating. Appl Phys Lett. 2024;125(4). doi:10.1063/5.0210841.
62. Machado P, Caño I, Menéndez C, Cazorla C, Tan H, Fina I, et al. Enhancement of phase stability and optoelectronic performance of BiFeO3 thin films via cation cosubstitution. J Mater Chem C. 2021;9(1):330-339. doi:10.1039/D0TC04304D.
63. Islam MZ, Hasan M, Rahman MF, Rhaman MM. DFT-based insights into Ca, Mg, and Cr-doped BaNpO3 perovskites for advanced optoelectronic applications. Next Mater. 2025;8:100538. doi:10.1016/j.nxmate.2025.100538.
64. Zemene S, Yohannes YB, Wubetu GA. Synthesis and characterization of undoped and Co-doped bismuth ferrite nanoparticles for photovoltaic applications. Phys Scr. 2025;100(1):0159a5. doi:10.1088/1402-4896/ad9eeb.
65. Shuvo AKMA, Adnan MMR, Islam MS, Rhaman MM. Influence of annealing temperature on the structural, dielectric, and impedance properties of Sm and Co co-doped BiFeO3 for advanced

electronic and energy applications. Next Mater. 2026;11:101967. doi:10.1016/j.nxmate.2026.101967.
66. Lei T, Cai W, Fu C, Ren H, Zhang Y, Sun Y, et al. The effects of grain size on electrical properties and domain structure of BiFeO3 thin films by sol-gel method. J Mater Sci Mater Electron. 2015;26(12):9495-9506. doi:10.1007/s10854-015-3690-z.
67. Ivanov MS, Khomchenko VA, Silibin MV, Karpinsky DV, Blawert C, Serdechnova M, et al. Investigation of local conduction mechanisms in Ca and Ti-doped BiFeO3 using scanning probe microscopy approach. Nanomaterials. 2020;10(5):940. doi:10.3390/nano10050940. PMID:32422891.
68. Sinha AK, Bhushan B, Jagannath RK, Sharma RK, Sen S, Mandal BP, et al. Enhanced dielectric, magnetic and optical properties of Cr-doped BiFeO3 multiferroic nanoparticles synthesized by sol-gel route. Results Phys. 2019;13:102299. doi:10.1016/j.rinp.2019.102299.
69. Taisan NA, Kumar S, Alshoaibi A. Structural, electrical and optical properties of TM (Mn and Cr) doped BiFeO3 nanoparticles. Crystals. 2022;12(11):1610. doi:10.3390/cryst12111610.
70. Wang N, Luo X, Han L, Zhang Z, Zhang R, Olin H, et al. Structure, performance, and application of BiFeO3 nanomaterials. Nano Micro Lett. 2020;12(1):81. doi:10.1007/s40820-020-00420-6. PMID:34138095.
71. Yin L, Mi W. Progress in BiFeO3-based heterostructures: Materials, properties and applications. Nanoscale. 2020;12(2):477-523. doi:10.1039/C9NR08800H. PMID:31850428.
72. Chen G, Chen J, Pei W, Lu Y, Zhang Q, Zhang Q, et al. Bismuth ferrite materials for solar cells: Current status and prospects. Mater Res Bull. 2019;110:39-49. doi:10.1016/j.materresbull.2018.10.011.
73. Lv J, Ning H. Photovoltaic effect of La and Mn co-doped BiFeO3 heterostructure with charge transport layers. Materials. 2024;17(9):2072. doi:10.3390/ma17092072. PMID:38730875.

